Antiferromagnetic ground state and evidence for metamagnetic transition in itinerant-electron compounds YCo12-xFexB6 (x = 1.5, 2, 2.5)

B. Vallet-Simond, L.V.B. Diop, O. Isnard

Antiferromagnetic ground state and evidence for metamagnetic transition in itinerant-electron compounds $YCo_{12-x}Fe_xB_6$ (x = 1.5, 2, 2.5)

B. Vallet-Simond[1], L. V. B. Diop[2], O. Isnard[1]
[1]*Université Grenoble Alpes, Institut Néel, CNRS, BP166X, 38042 Grenoble Cédex 9, France*
[2]*Université de Lorraine, CNRS, IJL, F-54000 Nancy, France*

Abstract

In contrast to the parent compound $YCo_{12}B_6$, the Fe-doped $YCo_{12-x}Fe_xB_6$ ($1.5 \leq x \leq 2.5$) alloys exhibit an antiferromagnetic ground state. It is further revealed that the antiferromagnetic state gets transformed into a forced ferromagnetic state by way of a magnetic-field-induced metamagnetic transition. The results demonstrate a progressive reinforcement of the antiferromagnetic interactions upon increasing Fe content along the $YCo_{12-x}Fe_xB_6$ series of compounds. The magnetic phase diagram of each (x = 1.5, 2 and 2.5) composition is determined by combining isothermal and isofield magnetization measurements. The composition and temperature dependencies of the critical field are derived and discussed. Whereas for x = 2 and 2.5 the magnetic state changes from antiferromagnetic (AFM) to ferromagnetic (FM) and then to the paramagnetic (PM) state upon heating, exhibiting three distinct temperature regions, a multicritical point of magnetic origin is proposed for the x = 1.5 compound at a temperature of about 117 K. The ordering temperature is found to decreases upon increasing Fe concentration while the critical field of the AFM-FM metamagnetic phase transition shows the opposite trend. The critical transition field diminishes upon increasing temperature.

Keywords: intermetallic compounds, itinerant electron metamagnetism, magnetic phase diagrams

I. Introduction

The itinerant-electron metamagnetism (IEM), i.e., the first-order field-induced transition from a low-magnetization state to a relatively high-magnetization state in itinerant-electron systems, is a very specific physical concept that describes magnetic properties of some intermetallic compounds. The IEM phenomenon demonstrates potentially important multifunctionalities such as the giant magnetocaloric effect (MCE), huge magnetostriction and colossal magnetoresistance [1-5]. The report of giant MCE in $La(Fe,Si)_{13}$ silicides [2] has

triggered a regain of interest for IEM compounds. Over the past 20 years, there has been worldwide a spectacular surge in research of materials with first order metamagnetic transitions. This has opened new perspectives for room temperature magnetic refrigeration. Metamagnetic materials are a key component of the solid-state-based magnetic refrigeration—an environmentally friendly promising alternative to conventional cooling technology.

A fascinating candidate to explore IEM is $LaFe_{12}B_6$ boride which occupies a special place among rare-earth iron-rich intermetallic systems. The physical properties of this metamagnet have been thoroughly studied, manifesting numerous intriguing distinctive features, anomalous and exotic magnetic behavior. Indeed, unconventional and discontinuous staircase-like metamagnetic transitions were observed in the magnetization isotherms of $LaFe_{12}B_6$ [6-9]. This unique and peculiar avalanche-like magnetization process consists of a succession of ultrasharp steps separated by plateaus. Neutron diffraction experiments in zero magnetic field have revealed an unusual amplitude-modulated antiferromagnetic spin configuration. This magnetic structure is defined by a wave vector $\mathbf{k}$ = (¼, ¼, ¼) and remarkably weak Fe magnetic moment of about 0.43 μ_B in the ground state [6]. Furthermore, the antiferromagnetic itinerant-electron system $LaFe_{12}B_6$ is characterized by an extraordinary low magnetic ordering temperature T_N = 36 K for an Fe-rich intermetallic compound and a multicritical point in the complex magnetic phase diagram with multiple step transitions [6]. $LaFe_{12}B_6$ displays colossal spontaneous magnetization jumps occurring after a very long incubation time in experimental conditions where external parameters (applied magnetic field and temperature) are kept constant [8], both inverse and conventional MCE [10], large hydrostatic pressure effects [11], huge negative thermal expansion and giant magnetostriction [5]. These prominent magnetoresponsive effects of relevance highlighted the potential interest of $LaFe_{12}B_6$ metamagnetic material in future low-temperature energy technologies, e.g., in a high performance cryogenic magnetostrictive actuator, and cryogenic magnetic cooling. They also stimulated the development of experiments under extreme conditions and theoretical models for a better understanding of the physics underlying the striking phenomenology of this intermetallic compound [11-15]. The Fe-rich itinerant-electron metamagnetic compound $LaFe_{12}B_6$ constitutes an exceptional playground for materials physics due to the extreme sensitivity of its physical properties to either chemical [9, 16, 17] or hydrostatic pressure [11].

Most recently, Diop and co-workers have reported the occurrence of a field-induced structure transformation across the metamagnetic phase transition in Ce-containing $(La,Ce)Fe_{12}B_6$ pseudo-ternary alloys [18-19], in other words, a first-order magnetostructural transformation or a coupled magnetic-crystallographic transition. This symmetry-lowering

lattice distortion converts the crystal structure from rhombohedral to monoclinic. The structural distortion is driven by magnetoelastic coupling and is accompanied by a remarkably large negative magnetoresistance of −73% [18]. The volume magnetostriction related to the crystallographic transition is estimated to be 0.9% in $La_{0.85}Ce_{0.15}Fe_{12}B_6$ [18]. The profound bonding, structural, magnetic, and electronic alterations, which take place in $(La,Ce)Fe_{12}B_6$, causes substantial changes of the materials' behavior leading to a rich assortment of strong magnetoresponsive physical phenomena. These experimental findings illustrate the strength of the coupling between lattice, charge, and spin degrees of freedom in the IEM system $(La,Ce)Fe_{12}B_6$.

In contrast to the rather complex magnetic behavior of $LaFe_{12}B_6$, the Co-based $RCo_{12}B_6$ isotype phases (R stands for a rare-earth atom) present more simple magnetism. The $RCo_{12}B_6$ borides are stable for essentially all the rare-earths, while $LaFe_{12}B_6$ is the unique stable Fe-based member of the 1-12-6 family. The lattice parameters for the $RCo_{12}B_6$ series of compounds follow the conventional lanthanide contraction [20]. They are all ferro- (R =Y, La-Sm) or ferri- (R = Gd-Tm) magnets with modest magnetic ordering temperatures (T_C =134 - 162 K) and a small mean Co magnetic moment (0.44 μ_B/Co in $YCo_{12}B_6$). The Curie temperature is weakly dependent on the rare-earth element. The low intrinsic magnetic properties of the $RCo_{12}B_6$ ternary compounds are attributed to the relatively small number of Co with respect to B (factor of 2) and to the hybridization of B(p) and Co(d) electrons bands as a result of short distances between B and Co atoms (≈ 2.05 Å). Study of the Co magnetic behavior of these alloys in both magnetically ordered and paramagnetic states has led to remarkably different values of Co magnetic moments in the ferromagnetic state ($\mu_{Co} \approx 0.44\ \mu_B$) and in the paramagnetic state ($\mu_{Co} \approx 1.76\ \mu_B$) [22]. This yields a number of spin $S_0 = 0.22$ and $S_p = 0.51$ in the magnetically ordered and disordered phase, respectively. The corresponding Rhodes-Wohlfarth ratio $r = S_p/S_0$ amounts to ≈ 2.32. This result demonstrates the itinerant character of the Co-sublattice magnetism in these compounds. Nuclear magnetic resonance (NMR) data and neutron diffraction analyses denote significantly different Co moments on the two transition metal crystal sites, with the Co(18*h*) magnetic moment being larger than the Co(18*g*) one [21-22]. This difference in the Co ordered magnetic moments is driven by the different local chemical environments, i.e., different nearest-neighbor configurations. $LaCo_{12}B_6$ exhibits an incommensurate conical magnetic structure with Co moments tilted 60° away from the threefold symmetry axis *c* [22]. It is noteworthy that, in the $RCo_{12}B_6$ series, $NdCo_{12}B_6$ and $HoCo_{12}B_6$ undergo a spin reorientation transition [23-27] resulting from the

competition between the magnetocrystalline anisotropies due to the Co and Nd/Ho sublattices which have different preferred direction. The role of volume changes on the Curie temperature and the spontaneous moment of $RCo_{12}B_6$ has been studied by magnetization measurements under hydrostatic pressure up to 1 GPa [22, 28-30]. Only moderate magnetovolume effects have been observed for all investigated alloys. A sharp Hopkinson peak was detected near the Curie point of the ferromagnetic $YCo_{12}B_6$ compound and interesting transport properties have been found to occur around such unusually large Hopkinson effect [31]. The electrical impedance results suggest that the Hopkinson peak originates from a critical phenomenon related to the initial permeability. Furthermore, remarkable electronic transport and magnetotransport properties have been reported for $RCo_{12}B_6$ (R = Y, Ho, and Gd) [32].

As discussed in our recent paper [33], the pseudo-ternary system $Y(Co,Fe)_{12}B_6$ adopts the rhombohedral $SrNi_{12}B_6$-type structure (space group R-3m #166) in which the Co/Fe atoms are located on two inequivalent Wyckoff positions (18*g* and 18*h*) with the B and Y atoms occupying the 18*h* and 3*a* crystal sites, respectively. It is shown that partial substitution of Fe for Co in $YCo_{12-x}Fe_xB_6$ series of compounds induces an anisotropic expansion of the lattice: the expansion rate along the high-symmetry direction *c* is smaller than that in the basal-plane. The solubility limit was established at $x = 4$ [33]. The evolution of the interatomic distances also indicated a progressive cluttering of the crystal lattice, hence the solubility limit. The magnetic studies demonstrated through several parameters, that AFM interactions were getting stronger with the Fe content. The Curie-Weiss temperature kept on decreasing until it reached a negative value for $x = 4$. Another element is the progressive decrease of the magnetic moment in the ordered state from 5.39 μ_B/f.u. for $x = 0$ to 1.32 μ_B/f.u. for $x = 4$. Two theoretical models were also used to probe this series of compounds. Kuz'min's model of ferromagnets, also strongly favoured the hypothesis of a progressive strengthening of the AFM interactions at the expense of the FM ones upon increasing Fe content [34]. The Inoue-Shimizu model, based on a Landau expansion of the free energy, proved that considering these compounds as ferromagnets was possible around T_C up to $x = 2.5$ [34]. As explained in Refs.33-34, ferromagnetic impurities are present, thus the magnetic signal processing is extremely sensitive to the percentage of each phase and the accurate shape of the ferromagnetic impurity's signal. Perfecting the magnetic correction led us to a discrepancy at low magnetic fields for magnetization isotherms of compounds with $x = 1.5$, 2, and 2.5. Measurements were reproduced with different magnetometers and high density of measurement points at low field, and thus, the metamagnetic transition of itinerant electrons was revealed. Here, we present

detailed results on these metamagnetic transitions and propose magnetic phase diagrams for those compounds.

II. Experimental techniques

The samples employed in the present study were taken from the same batches as those used previously in Ref. 33. Details on the synthesis and subsequent characterization of the pseudo-ternary $YCo_{12-x}Fe_xB_6$ alloys are reported elsewhere [33].

The magnetic measurements have been performed using an extraction-type magnetometer that has been described elsewhere [35,36]. This equipment enables to perform magnetization measurements in the temperature range from 2 to 300 K and in applied magnetic fields of up to 10 T. The presence of minority (Fe,Co) boride phase has been identified by X-ray diffraction and its magnetic contribution removed from the magnetization curves by using the Honda-Owen method [33, 34, 37] in order to extract the intrinsic magnetic properties of the main $YCo_{12-x}Fe_xB_6$ phase. The amount of impurity present has been determined by two methods: (i) Rietveld analysis of the X-ray diffraction patterns and (ii) magnetization measurements [33]. In order to have the best correction possible, we measured the ferromagnetic impurity signal with great details at temperatures close to 250 K, where our main phase would be purely paramagnetic. As the T_C of the impurity is above 600 K [38], the shape of the magnetization curve is stable form 250 K to 2 K. From the detailed data on the (Fe,Co) [38-41] borides, we know the magnetization's evolution in this temperature range and can thus subtract the impurity ferromagnetic signal to the $Y(Co,Fe)_{12}B_6$ phases. The correction to the sample mass is done with the help of precise Rietveld refinement (described in [33]) as the Honda-Owen method is hardly applicable with more than one FM impurity.

III. Results and discussion

III.a. Metamagnetism in $YCo_{12-x}Fe_xB_6$ (x = 1.5, 2, 2.5)

In order to elucidate the magnetic states at different temperatures and applied fields, magnetization isotherms were recorded on the zero-field cooled $YCo_{12-x}Fe_xB_6$ samples. The initial magnetization data and the corresponding subsequent envelope loop at 2 K for $YCo_{10}Fe_2B_6$ are plotted in Figure 1. The virgin curve exhibits a sharp field-induced metamagnetic phase transition from the AFM ground state to the forced FM state. This metamagnetic transformation proceeds through a gradual conversion of the AFM phase into fully FM polarized domains upon rising external field. The field-driven AFM-FM phase transformation is completely reversible, and the compound recovers the original AFM state

when the applied magnetic field is reduced to zero. In other words, the induced-FM phase loses its stability after removal of the external field. The hysteresis cycle is symmetric as it can be distinctly seen from Figure 1. Another salient feature is that the hysteresis loop shows neither remanent magnetization nor coercivity. This result is consistent with the interpretation of an AFM ground state and as well as with the reversible behaviour of the field-induced transformation. The saturation magnetization of the forced FM state is estimated to be 4.45 μ_B/f.u. at 2 K: leading to a mean magnetic moment of 0.37μ_B per 3*d* transition metal atom.

Figure 2 displays the isothermal magnetization curve for $YCo_{10.5}Fe_{1.5}B_6$ measured at 20 K. The metamagnetic transition reported in Figure 2 is remarkable in two ways: (i) by the large magnetization variation and (ii) by the existence of a clear magnetic hysteresis against the field scan, which bears witness to the first-order nature of the transition. The critical field of the metamagnetic transition is determined from the peak position of the first derivative of magnetization with respect to the magnetic field (inset of Figure 2). At 20 K, the critical magnetic transition field amounts to 0.26 T and 0.21 T for the ascending-field branch and the reverse leg, respectively. This corresponds to a hysteresis width of 0.05 T. It is worth recalling that the value of the critical field $\mu_0 H_{cr}$ is related to the free-energy difference ΔF between the FM and AFM states as $\Delta F \approx M_{cr} \cdot \mu_0 H_{cr}$ [42]. Here M_{cr} represents the magnetization at the transition field $\mu_0 H_{cr}$. The observed AFM-FM metamagnetic transition strongly implies that the magnetic free-energy of $YCo_{10.5}Fe_{1.5}B_6$ has a double minimum associated with the AFM and FM phases. Therefore, the thermodynamic state moves from the local minima in the AFM state to the local minima in the FM state separated by an energy barrier in the magnetic free energy.

Similar metamagnetic transition is also observed for x = 2.5 as exemplified in Figures 3 and 4, in which we compare the magnetization isotherms recorded at temperatures of 2 and 20 K for three compositions (x = 1.5, 2, and 2.5). One remarks that, the AFM-FM metamagnetic transformation is shifted toward higher magnetic fields upon increasing Fe concentration. In addition, the width of the field hysteresis progressively diminishes upon heating. Some differences can be seen in the magnetic moment with respect to the Fe content.

Unlike the compounds with x = 0, 0.5 and 1 reported elsewhere [34], which present a conventional ferromagnetic-like behaviour, the x = 1.5, 2 and 2.5 compositions studied here exhibit an AFM ground state that can be converted into a forced FM state by way of a field-induced transition. A result that has not been reported to date. The reason for which this phenomenon was not discovered before is most probably due to the presence of ferromagnetic impurities (Fe or $(Fe,Co)_2B$) masking the signal of the $RM_{12}B_6$ crystal phase. Indeed, such

often reported ferromagnetic impurities can hide the much weaker antiferromagnetic signal of the main $YCo_{12-x}Fe_xB_6$ phase. The careful correction for the impurity contribution to the magnetization curves carried out in the present study enables to extract the intrinsic magnetic properties of the $YCo_{12-x}Fe_xB_6$ series of compounds. Consequently, revealing their antiferromagnetic ground state and an AFM to FM transition. It is worth to recall the progressive reduction of the Curie-Weiss temperature which becomes even negative along the $YCo_{12-x}Fe_xB_6$ series of compounds [34] this also plays in favour of the AFM ground state deduced here from low temperature magnetization curves.

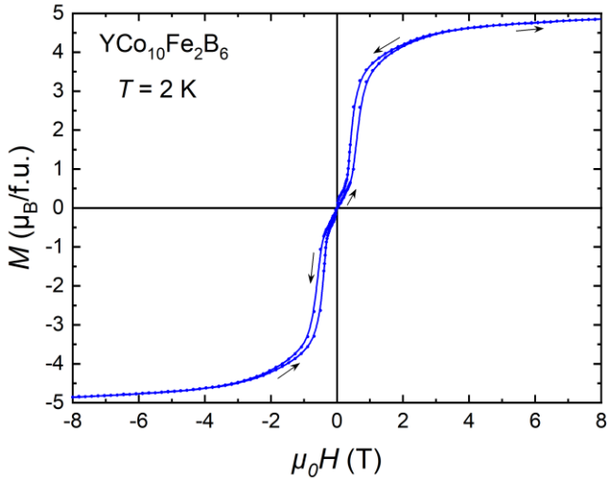

Figure 1: Hysteresis loop of $YCo_{10}Fe_2B_6$ at T = 2 K. The arrows denote the field directions in which measurements have been performed.

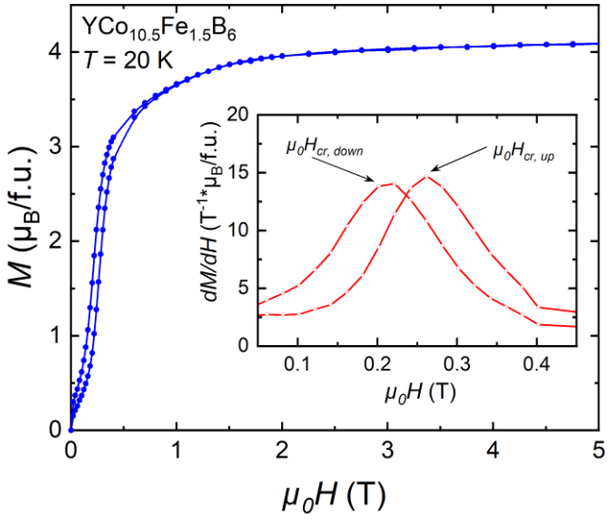

Figure 2: Magnetization isotherm of $YCo_{10.5}Fe_{1.5}B_6$ measured at T = 20 K. The inset shows the field derivative curve.

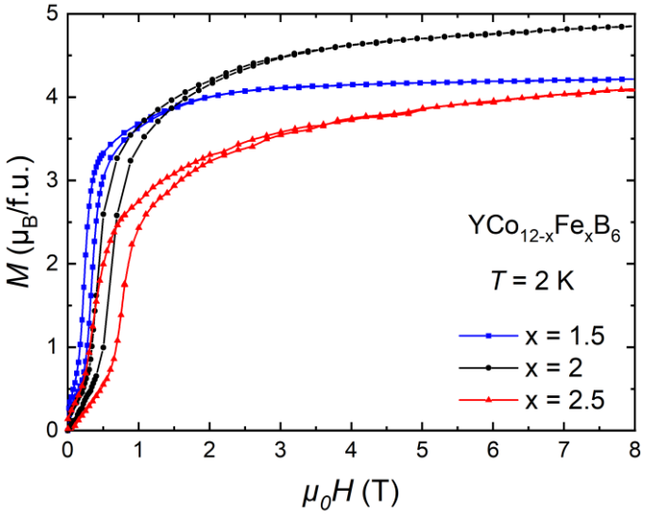

Figure 3: Magnetization isotherms of $YCo_{12-x}Fe_xB_6$ at T = 2 K.

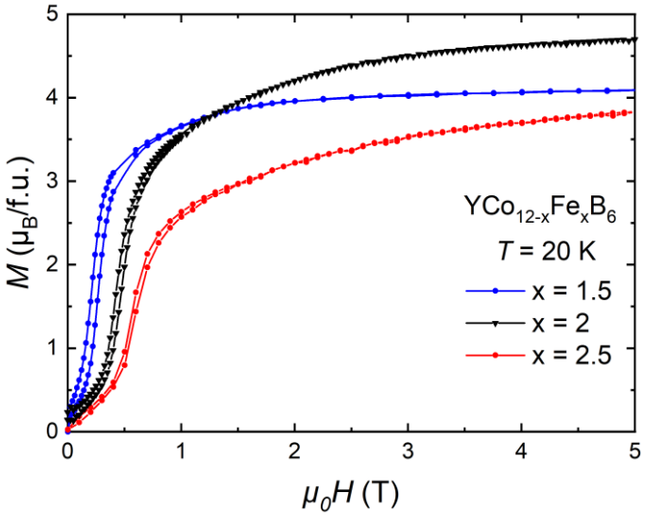

Figure 4: Magnetization isotherms of $YCo_{12-x}Fe_xB_6$ at T = 20 K.

III.b. Magnetic phase diagrams of $YCo_{12-x}Fe_xB_6$ (x = 1.5, 2, 2.5) compounds

Many isothermal magnetization curves have been recorded up to the magnetic ordering temperature for all three compositions x = 1.5, 2, 2.5 studied in the present work. The critical magnetic transition field was deduced from these *M(H)* curves as previously described (see inset of Figure 2) and all the recorded magnetization data were used to construct their magnetic phase diagrams. The critical field of the first magnetization curve is plotted in Figure 5 as a function of temperature for the three investigated compounds (x = 1.5, 2, and 2.5). The critical field is maximum at 2 K and decreases regularly upon heating, then vanishing at the Néel temperature estimated to be about 127, 95 and 75 K for x = 1.5, 2 and 2.5, respectively. At 2 K, the critical field is much larger for the compounds richer in Fe. This clearly demonstrates

the major role of Fe atoms within the crystal lattice and can be interpreted as reflecting the tendency of Fe-Fe exchange interactions to be of AFM type for short interatomic distances such as the one observed in $YCo_{12-x}Fe_xB_6$ crystal structures. The critical field is 0.77 T, twice larger for the x = 2.5 than for the x = 1.5 compound. This bears witness to the fact that AFM ordering is more stable upon increasing Fe content.

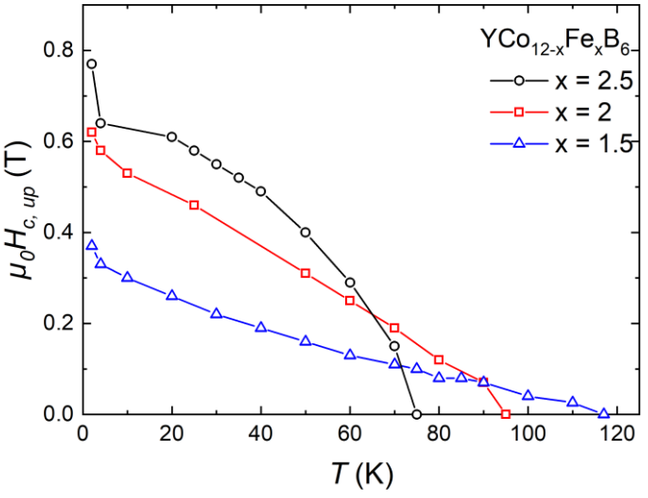

Figure 5: Critical magnetic transition field for $YCo_{12-x}Fe_xB_6$. Here, all the fields were measured in the first magnetization curve after zero-field cooling.

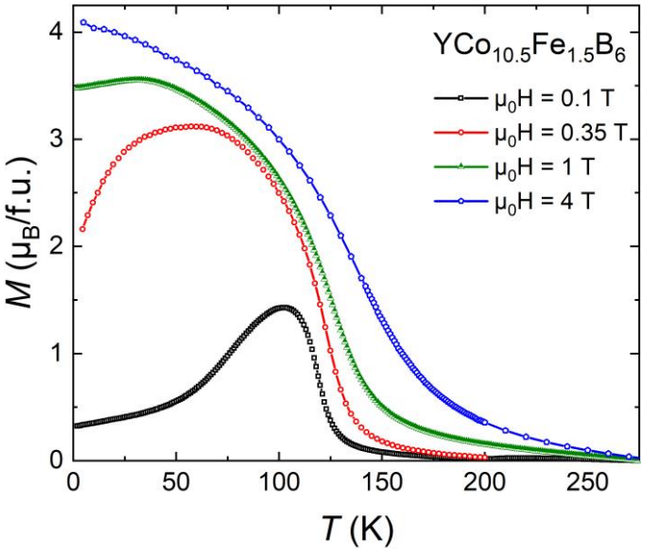

Figure 6: Temperature dependence of the isofield magnetization curves recorded at the indicated field values for $YCo_{10.5}Fe_{1.5}B_6$.

The thermomagnetic curves *M(T)* of $YCo_{10.5}Fe_{1.5}B_6$, measured under various applied fields, are depicted in Figure 6. The isofield magnetization curves collected in 0.1 and 0.35 T (low field) present a transition with an upturn in magnetization upon increasing temperature

reflecting the change from AFM (low magnetization) to FM behaviour in the intermediate temperature range. Then, when increasing temperature further, a strong decrease in magnetization occurs near the Curie point indicating a transition to the paramagnetic state. Such bell-like shape of the low-field thermomagnetic curves is similar to that reported for isostructural $LaFe_{12}B_6$ compound [6-7] recently identified as an itinerant-electron antiferromagnet with huge staircase-like metamagnetic transitions and remarkable magnetoresponsive physical properties [5, 7]. However, the bell-shaped behaviour occurs at much higher fields in $LaFe_{12}B_6$, namely, within the magnetic field range from 4.75 to 7 T. This similarity may be taken as a clue that interesting physical properties may be also discovered in the $YCo_{12-x}Fe_xB_6$ compounds.

As expected, when the applied field exceeds the critical field value ($\mu_0 H$ = 1 and 4 T) $YCo_{10.5}Fe_{1.5}B_6$ behaves as a pure ferromagnet from the lowest temperature (2 K) up to the Curie temperature – Figure 6. Temperature values of 137 K and 159 K have been estimated for T_C under an applied magnetic field of 1 and 4 T, respectively. This corresponds to a dT_C/dH of 6.1 K/T for $YCo_{10.5}Fe_{1.5}B_6$. $YCo_{10}Fe_2B_6$ compound also presents similar behaviour of its isofield magnetization but with a sensitivity dT_C/dH= of 5.9 K/T. Similar values of dT_C/dH are expected for x=2.5 but thermomagnetic curve has been measured above $\mu_0 H$ = 1 T. These results have been used to plot the black lines in the magnetic phase diagrams in Figure 7, 8 and 9.

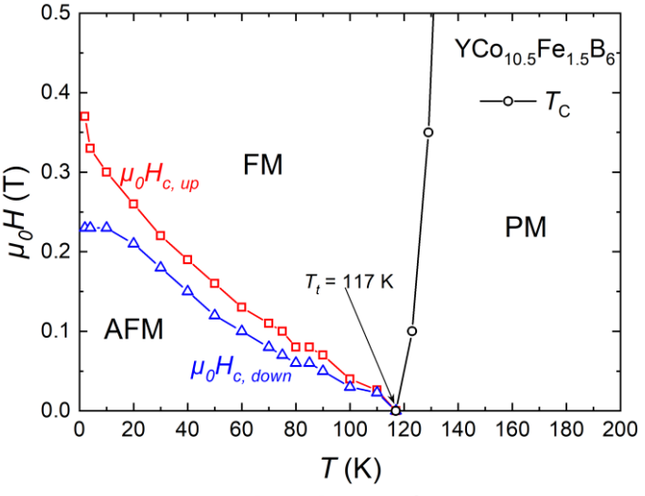

Figure 7: Magnetic phase diagram for $YCo_{10.5}Fe_{1.5}B_6$.

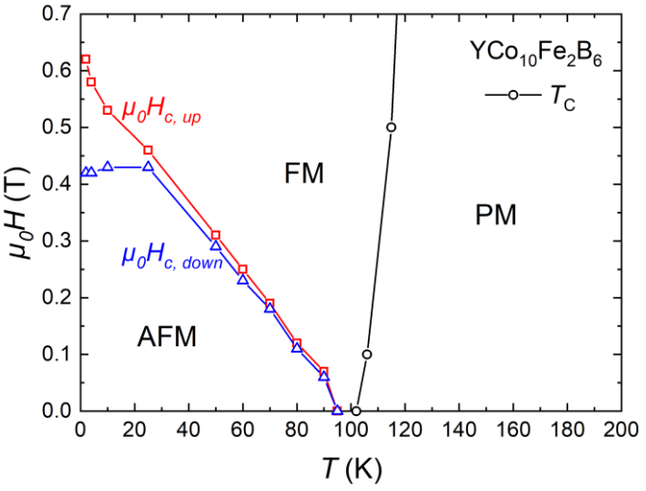

Figure 8: Magnetic phase diagram for $YCo_{10}Fe_2B_6$.

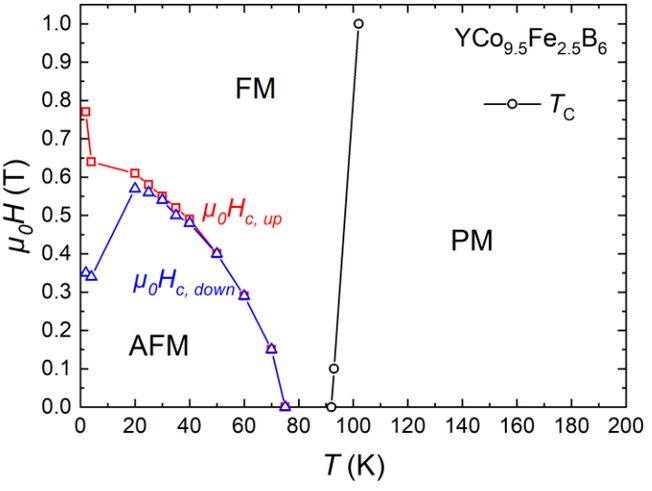

Figure 9: Magnetic phase diagram for $YCo_{9.5}Fe_{2.5}B_6$.

Using the critical field determined from isothermal magnetization curves, we have constructed the magnetic phase diagram plotted in Figures 7, 8 and 9. As can be seen in the magnetic phase diagram of $YCo_{10.5}Fe_{1.5}B_6$ compound, 117 K can be regarded as a critical temperature where the AFM, FM and PM states coexist. That is to say a multicritical point. In the other two compounds (x = 2 and 2.5) the critical temperature between the AFM state and the FM state is separated from the Curie temperature of the transition between the FM state and the PM state. The temperature gap ΔT between both transition temperatures increases upon increasing the Fe content. The values corresponding to each composition are listed in Table 1 and plotted against Fe concentration in Figure 10.

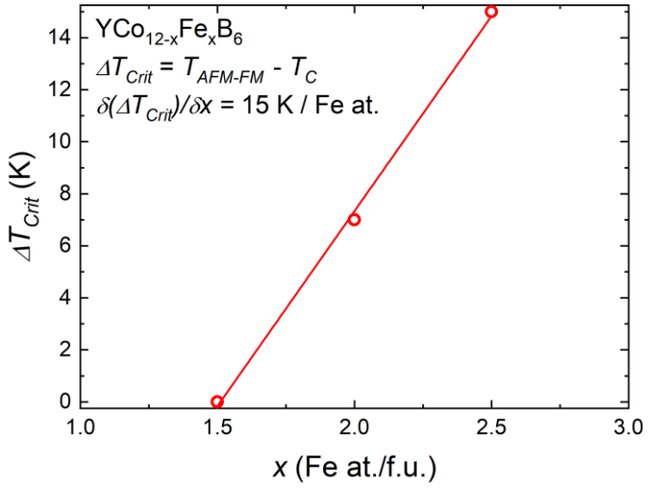

Figure 10: Composition dependence of the difference between T_C and T_{AFM-FM}

x (Fe at./f.u.)	m_{3d} (μ_B/$_{3d}$) = q_s	m_{eff} (μ_B)	T_{AFM-FM} (K)	T_C (K)	ΔT_{Crit} = T_{AF-F}-T_C (K)
1.5	0.34	1.87	117(3)	117(3)	0
2	0.37	2.04	95(3)	102(3)	7
2.5	0.28	2.20	75(3)	92(3)	15

Table 1: Magnetic properties of the $YCo_{12-x}Fe_xB_6$ compounds studied here x = 1.5 to 2.5 as determined in the ordered and paramagnetic state. Transition temperature observed in the magnetic phase diagram of $YCo_{12-x}Fe_xB_6$ series of compounds, T_{AFM-FM} stand for the AFM to FM state transition under zero applied field, T_C for the Curie temperature, and ΔT_{Crit} for the difference between the two.

The transition from AFM to FM is as expected of first-order type with a measurable filed hysteresis in the magnetization curves. It is worth to point out that the difference between the critical field measured for the upward ($\mu_0 H_{c,up}$) and downward ($\mu_0 H_{c,down}$) field variation is much larger below 20 K. This is easily seen in Figure 1 for $YCo_{10.5}Fe_{1.5}B_6$ where $\mu_0 H_{c,down}$ = 0.23 T at 2 K. In a similar manner $YCo_{10}Fe_2B_6$ compound is exhibiting a saturation of $\mu_0 H_{c,down}$ at 0.42 T at low temperature (below 30 K) whereas $\mu_0 H_{c,up}$ continuously increases as the temperature is lowered. The width of the hysteresis observed across the AFM-FM metamagnetic transition is found to be maximal for x = 2.5, below T = 20 K (see Figure 9). However, above T = 20 K, the general trend is that the Fe content causes a reduction of the hysteresis from x = 1.5 to 2.5. The low temperature critical field strength is very composition dependent as follows from Figure 11, $\mu_0 H_{crit}$ increases monotonically with Fe concentration ($d\mu_0 H_{c,up}/dx$ = 0.4 T/Fe atom). Due to the presence of larger content of ferromagnetic impurity phase as well as the proximity to the solubility limit [33], compositions with $x \geq 3$ have not been investigated. In addition, the lower magnetization of these 1:12:6 phases with high Fe

content is a further difficulty encountered. It is worth to mention that some hysteresis was observed at low field and low temperature, but the magnitude of the magnetic moment was so weak and the impurity correction too big, the end data was extremely noisy.

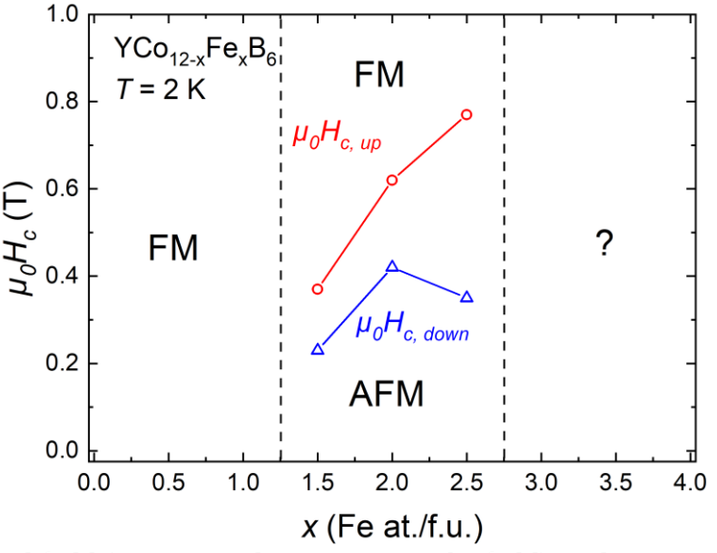

Figure 11: Critical field (as measured on increasing the field) evolution with the chemical composition at T = 2 K.

IV. Conclusion

Isothermal as well as isofield magnetization measurements have been carried out on the $YCo_{12-x}Fe_xB_6$ series of compounds. Our detailed study to extract the intrinsic magnetic properties reveals that an AFM ground state is observed for x = 1.5 to 2.5. The low-field thermomagnetic curves exhibit a bell-shaped feature correlated with the existence of three distinct magnetic phase domains: AFM at low temperatures then field-induced FM at the intermediate temperatures and PM state at higher temperatures. The studied compounds with x = 1.5 , 2 and 2.5 display interesting behaviour at the verge between the FM and AFM state. This leads to a complex magnetic phase diagram which shows two transition temperatures as well as critical fields typical of metamagnetic transitions. The magnetic properties are found to be very senstivive to the Fe content. The compounds with $x \leq 1$ are known to present a ferromagnetic-like ground state whereas, for $1.5 \leq x \leq 2.5$ the ground state becomes antiferromagnetic. The choise of iron content is a manner to tune the critical field of the metamagnetic transition between the AFM and FM states. A sensitivity of $d\mu_0 H_{c,up}/dx$ = 0.4 T/Fe atom is determined at 2 K. A Critical magnetic transition field as high as 0.77 T is obtained for x = 2.5. Whereas the x = 2 and 2.5 composition exhibit distinct critical temperatures, they

merge for $YCo_{10.5}Fe_{1.5}B_6$ compound leading to a multicritical point. For x = 2 and 2.5 composition a FM domain is observed between the AFM and PM one.

The discovery of this AFM ground states for x = 1.5 to 2.5 on polycrystalline samples here is worth to be investigated further for instance on single crystalline samples in order to probe the magnetic properties along the principal crystallographic directions. In addition neutron diffraction study would be interesting to reveal the magnetic structure of these compounds at the atomic scale.

Author Declaration Section

Conflict of Interest Statement:

The authors have no conflict to disclose.

Author Contributions:

Baptiste Vallet-Simond: Writing – original draft (equal); Formal Analysis (lead); Writing – review and editing (equal); Investigation (equal). Léopold V. B. Diop: Conceptualization (lead); Supervision (equal) - Writing – original draft (equal); Writing – review and editing (equal); Investigation (equal); Project Administration (equal). Olivier Isnard: Conceptualization (equal); Supervision (equal) -Writing – original draft (equal); Investigation (equal); Project Administration (lead).

Data Availability

The data that supports the findings of this study are available from the corresponding author upon reasonable request.

References:

[1] D.P. Kozlenko, E. Burzo, P. Vlaic, S.E. Kichanov, A.V. Rutkauskas, and B.N. Savenko, Sci. Rep. **5**, 8620 (2015).

[2] A. Fujita, S. Fujieda, Y. Hasegawa, and K. Fukamichi, Phys. Rev. B **67**, 104416 (2003).

[3] H. Yamada, and T. Goto Phys. Rev. B **68**, 184417 (2003).

[4] N.H. Duc, D.T. Kim Anh, and P.E. Brommer, Physica B **319**, 1 (2002).

[5] L. V. B. Diop, J. Prokleška, and O. Isnard, Appl. Phys. Lett. **122**, 192402 (2023).

[6] L.V. B.Diop, O. Isnard, and J. Rodrıguez-Carvajal, Phys. Rev. B **93**, 014440 (2016).

[7] S. Fujieda, K. Fukamichi, and S. Suzuki, J. Magn. Magn. Mater. **421**, 403 (2017).

[8] L. V. B. Diop and O. Isnard, Appl. Phys. Lett. **108**, 132401 (2016).

[9] L. V. B. Diop and O. Isnard, Phys. Rev. B **97**, 014436 (2018).

[10] L.V.B. Diop, and O. Isnard, J. Appl. Phys. **119**, 213904 (2016).

[11] L.V.B. Diop, O. Isnard, Z. Arnold, J.P. Itié, J. Kastil, and J. Kamarad, Solid State Comm. **252**, 29 (2017).

[12] G. I. Miletic and Z. Blazina, J. Magn. Magn. Mater. **323**, 2340 (2011).

[13] G. I. Miletic and Z. Blazina, J. Alloys Compd. **430**, 9 (2007).

[14] M. Rosenberg, T. Sinnemann, M. Mittag, and K. H. J. Buschow, J. Alloys Compd. **182**, 145 (1992).

[15] Q. A. Li, C. H. de Groot, F. R. de Boer, and K. H. J. Buschow, J. Alloys Compd. **256**, 82 (1997).

[16] X. Chen, Y. Mudryk, A.K. Pathak, and V.K. Pecharsky, J. Alloys Compd. **884**, 161115 (2021).

[17] Z. Ma, X. Dong, Z. Zhang, and L. Li, J. Mater. Sci. Technol. **92**, 138 (2021).

[18] L.V.B. Diop, T. Faske, O. Isnard, and W. Donner, Phys. Rev. Mater. **5**, 104401 (2021).

[19] L.V.B. Diop, T. Faske, M. Amara, D. Koch, O. Isnard, and W. Donner, Phys. Rev. B **104**, 134412 (2021).

[20] M. Mittag, M. Rosenberg, and K.H.J. Buschow, J. Magn. Magn. Mater. **82,** 109 (1989).

[21] M. Kawakami, and S. Satohira, J. Magn. Magn. Mater. **104**, 1313 (1992).

[22] L.V.B. Diop, Z. Arnold, O. Isnard, and J. Kamarád. J. Alloys Compd. **593**, 163 (2014).

[23] Z. Ma, P. Xu, J. Ying, Y. Zhang, and L. Li, Acta Mater. **247**, 118757 (2023).

[24] F. Mesquita, L.V.B. Diop, and O. Isnard, J. Alloys Compd. **763**, 355 (2018)

[25] J.M. Cadogan, S.J. Campbell, X.L. Zhao, and E. Wu, Aust. J. Phys. **46**, 679 (1993).

[26] L.V.B. Diop, and O. Isnard, J. Phys. Condens. Matter **27**, 026004 (2015).

[27] J.M. Cadogan, S.J. Campbell, X.L. Zhao, H.S. Li, and P.W. Thompson, Hyperfine interactions, in: M.F. Thomas, J.M. Williams, T.C. Gibb (Eds.), Proc., vol. **5**, pp. 119-122 (2002).

[28] Z. Arnold, O. Isnard, H. Mayot, M. Mísek, and J. Kamarád, J. Magn. Magn. Mater. **322**, 1117 (2010).

[29] Z. Arnold, O. Isnard, H. Mayot, Y. Skorokhod, J. Kamarád, and M. Mísek, Solid State Commun. **152**, 1164 (2012).

[30] L.V.B. Diop, Z. Arnold, J. Kamarád, and O. Isnard, J. Magn. Magn. Mater. **476**, 106 (2019).

[31] F. Mesquita, L.V.B. Diop, G. Fraga, O. Isnard, and P. Pureur, IEEE Magn. Lett. **6**, 3800304 (2015).

[32] F. Mesquita, S. G. Magalhaes, P. Pureur, L. V. B. Diop, and O. Isnard, Phys. Rev. B **101**, 224414 (2020).

[33] B. Vallet-Simond, S. Giron, L.V.B. Diop, and O. Isnard, J. Alloys Compd. **926**, 166700 (2022).
[34] B. Vallet-Simond, L.V.B. Diop, and O. Isnard, J. Magn. Magn. Mater. **587**, 171307 (2023)
[35] A. Barlet and J. C. Genna and P. Lethuillier, Cryogenics **31**, 801-805 (1991).
[36] A. Barlet and J. C. Genna and P. Lethuillier, Rev. Sci. Ins. **62**, 1824-1827 (1991).
[37] L.F. Bates, Modern Magnetism., p133. Cambridge University Press, Cambridge, England (1951).
[38] Landolt-Börnstein New Series IV/5. Springer-Verlag Berlin, Heidelberg (1980)
[39] A. Edström, M. Werwiński, D. Iuşan, J. Rusz, O. Eriksson, K. P. Skokov, I. A. Radulov, S. Ener, M. D. Kuz'min, J. Hong, M. Fries, D. Yu. Karpenkov, O. Gutfleisch, P. Toson, and J. Fidler, Phys. Rev. B, **92**, 174413 (2015); Erratum Phys. Rev. B **93**, 139901 (2016).
[40] T. N. Lamichhane, O. Palasyuk, V. P. Antropov, I. A. Zhuravlev, K. D. Belashchenko, I. C. Nlebedim, K. W. Dennis, A. Jesche, M. J. Krammer, S. L. Bud'ko, R. W. McCallum, P. C. Canfield and V. Taufour, J. Magn. Magn. Mater. **513**, 167214 (2020).
[41] D. Fruchart, P. Chaudouet, R. Fruchart, A. Rouault and J. P. Sénateur, J. Solid State Chem. **51**, 246-252 (1984).
[42] K. Irisawa, A. Fujita, K. Fukamichi, M. Yamada, H. Mitamura, T. Goto, and K. Koyama, Phys. Rev. B **70**, 214405 (2004).